Ultrasensitive Terahertz Nano-Probing for Semiconductors Using Nanogap Structures

Young-Mi Bahk[1] *and Minah Seo*[2,3]

[1] *Department of Physics, Incheon National University, Incheon, Republic of Korea*
[2] *Sensor System Research Center, Korea Institute of Science and Technology, Seoul, Republic of Korea*
[3] *KU-KIST Graduate School of Converging Science and Technology, Korea University, Seoul, Republic of Korea*

Abstract

There has been a growing interest in exploring novel opto-electrical behaviors and response of carriers under nonequilibrium conditions in semiconductor nanoscale materials for applications of photocurrent and operation of photodetectors. Terahertz waves have shown substantial promise for these applications, with the merit of direct observation of transient carrier dynamics and conductivity changes in semiconductor materials. Especially, to investigate surface carrier dynamics of such nanoscale semiconductor materials under photoexcitation, one can use nanosized materials such as nanofilms, nanowires, and nanoparticles, which have a very large surface-to-volume ratio. In this article, we introduce ultrafast phenomena in semiconductors investigated by terahertz probes. In particular, recent studies on how to observe carrier dynamics in a semiconductor with a spatial resolution of nanoscale levels below the diffraction limit of terahertz wave, using well-tailored metallic nanogap structures are mainly introduced. Metallic nanostructures having the ability to confine electromagnetic waves in a volume much smaller than wavelength play an important role in many application areas such as subwavelength waveguides, metamaterials, biochemical sensing, and photovoltaic technology. Strong local electromagnetic field confinement and enhancement accompanied by metallic nanostructures including nanogaps and nanotips have been widely used to manipulate interaction between electromagnetic waves and target materials. In addition to their diverse applications, their fundamental importance has received a great deal of attention in nano-optics and nano-photonics. The tunability of resonances by the geometrical effect of metal nanostructures can be exploited to increase the interaction efficiency between the nanostructures and electromagnetic waves at specific wavelength regions of interest.

Keywords *terahertz metamaterials; optical pump terahertz-probe spectroscopy; metallic nanogap; field localization; carrier dynamics*

Encyclopedia of Applied Physics.

DOI: http://dx.doi.org/10.1002/3527600434.eap839

1 Optical Pump Terahertz-Probe Spectroscopy

Terahertz waves are electromagnetic waves within frequencies from 0.1 to 100 THz (1 THz = 10^{12} Hz, $\lambda = 300\,\mu m$ at $f = 1$ THz) that locate between infrared and microwaves. Following the report by Ch. Fattinger and D. Grischkowsky on generation and detection of coherent terahertz waves using photoconductive antennas, there is great interest research on using terahertz time-domain spectroscopy system [1–5]. In the terahertz time-domain spectroscopy system, based on the short pulse of terahertz radiation, both amplitude and phase information of terahertz pulses can be measured, facilitating the investigation of complex optical constants of various materials [3, 5–10]. Furthermore, the radiation at terahertz frequencies is non-ionized due to low photon energy ($E \sim 4$ meV for 1 THz), thereby making terahertz spectroscopy attractive as a nondestructive examination tool [11–14].

In order to create terahertz pulses, a continuous wave (CW) green laser ($\lambda = 532$ nm) pumps Ti : sapphire crystals [Titanium-ion doped sapphire crystal ($Ti^{3+} : Al_2O_3$)] to generate ultrashort pulses with a pulse duration around 100 fs and a repetition rate of 80 MHz at a wavelength near 800 nm. The mode-locked optical pulse is guided and split into two parts: one is used for generation and the other for detection of terahertz pulses (Figure 1a). Typically, low-temperature grown GaAs crystals are used for photoconductive antennas in which charge carriers created by ultrashort pulse lasers are accelerated by the external bias voltage and generate polarized terahertz pulses. The generated terahertz pulses are guided by a series of parabolic mirrors from the emitter to the sample and then to the detector. Two types of detection methods are commonly used for terahertz time-domain spectroscopy: photoconductive antenna and electro-optical sampling in which low-temperature grown GaAs and electro-optical crystals such as ZnTe are used, respectively. In both cases, one beam of optical pulse laser is used in a time-gated manner for detection. By scanning the delay line, the electric field of terahertz pulse can be measured as a function of time with both amplitude and phase information (Figure 1b), and can be transformed into a frequency-domain spectrum after Fourier transformation (Figure 1c).

Optical pump terahertz-probe spectroscopy system can be built on terahertz time-domain spectroscopy by adding one more beam splitter, and then the optical pulse beam is divided into total three paths – (i) optical pump pulse, (ii) terahertz generation pulse, and (iii) detection pulse (Figure 1d). The optical pump path is controlled by a mechanical delay stage for the time interval between the optical pump pulse and terahertz probe pulse. By fixing the terahertz pulse path and scanning the optical pump path, the changes in the terahertz transmission through the sample at the peak field can be monitored as a function of pump-probe time delay. When the optical pump path is fixed and the terahertz pulse path is scanned, the transmitted terahertz waveforms are monitored, which allows one to extract the terahertz conductivity of materials.

In an optical pump scanning type in which a single point of the terahertz waveform is monitored as the optical pump delay is moved, the excited state dynamics of the sample can be investigated as a function of time delay after photoexcitation event [15–19]. This enables understanding diverse charge carrier dynamics in a sub-picosecond resolution because the transmission of the terahertz field is sensitive to the absorption of free charge carrier and bound charges with low energy such as excitons [15]. The other method, in which the entire terahertz waveform transmitted through the excited sample at various delays after photoexcitation, allows us to investigate the evolution of the frequency-dependent conductivity of the excited sample [20, 21]. After extraction of the conductivity, various conductivity

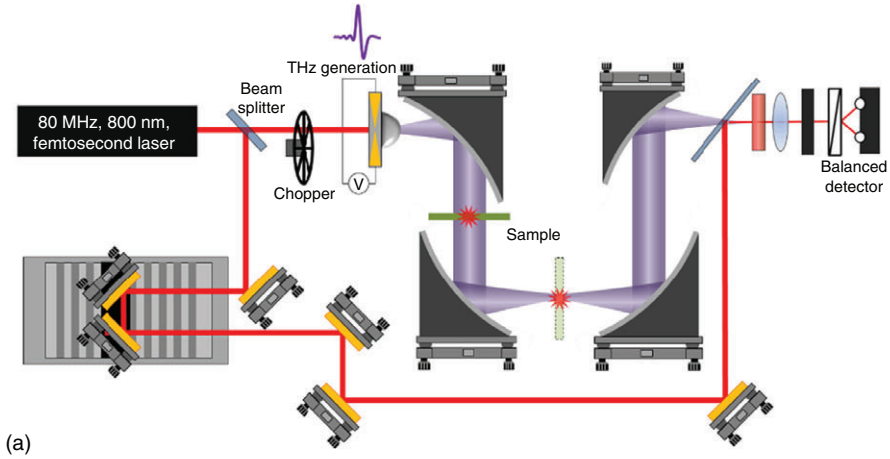

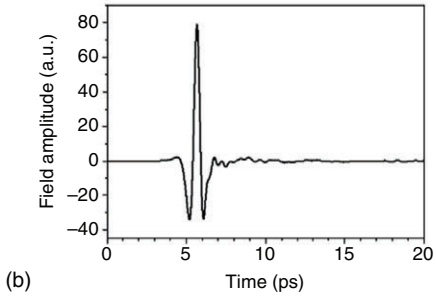

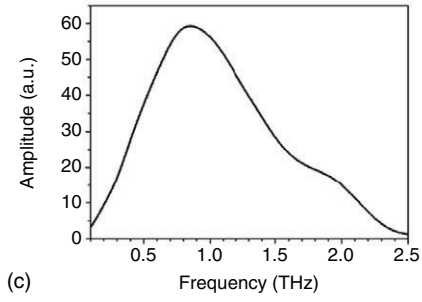

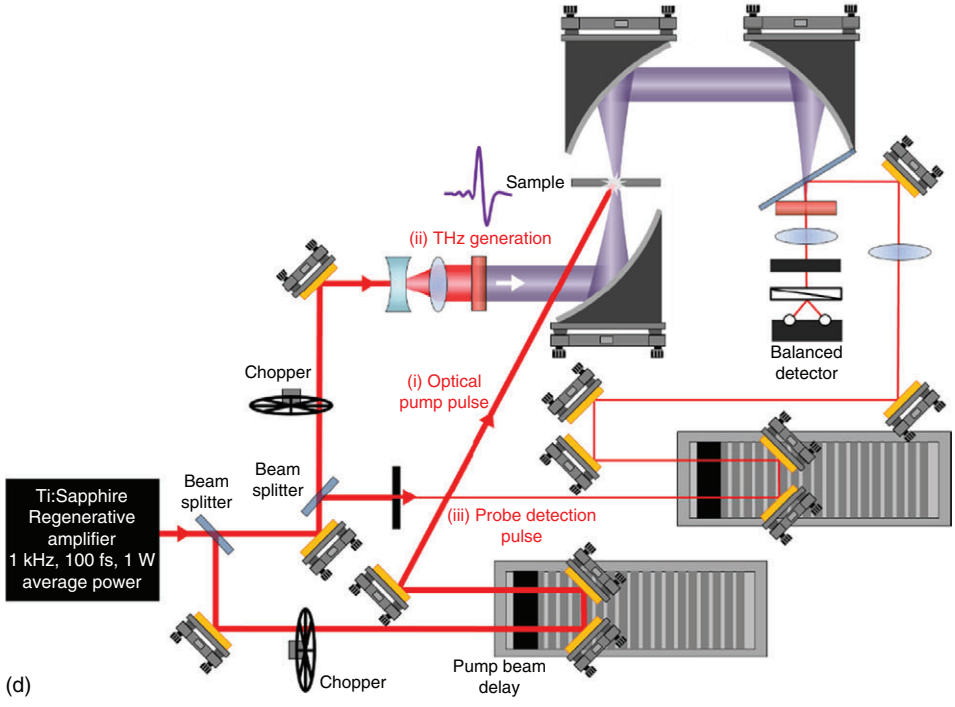

Figure 1 A typical terahertz time-domain spectroscopy setup (a), terahertz pulse in time domain (b), and Fourier-transformed spectrum (c). A typical optical pump terahertz-probe spectroscopy setup (d).

models are applied to examine the excited state dynamics. For charge carrier response, Drude-like model is typically used to estimate the carrier scattering and carrier density, while bound charge oscillation can be modeled to estimate the exciton polarizability and binding energy for the excitonic response.

2 Ultrafast Carrier Dynamics in Semiconductors

2.1 Ultrafast Carrier Dynamics in Bulk Semiconductors

Measurement of carrier dynamics of semiconductors is greatly important for the understanding of nonequilibrium phenomena such as carrier–carrier and carrier–phonon interactions occurring in materials [18, 22–25]. The capability to characterize transient photoconductivity in a noncontact fashion with a temporal resolution of the sub-picosecond scale is essential in the field of optoelectronics and nanoscale electronics. Time-resolved terahertz spectroscopy is a noncontact electrical probe that enables the measurement of the actual conductivity of photoexcited carriers even with a low density such as $5 \times 10^{10}\,\mathrm{cm}^{-2}$ in GaAs due to its high sensitivity. Transient electrical conductivity for nonequilibrium photoexcited carriers by a sub-picosecond laser pulse in GaAs was reported [22, 25–27]. Mobility change after photoexcitation with varying the initial kinetic energy of charge carriers was investigated. When the initial electron kinetic energy is an integral multiple of the longitudinal-optical (LO) phonon energy, then the frequency-dependent conductivity shows tremendous variations and oscillation within a few picoseconds after photoexcitation. When the initial kinetic energy is a half-integral multiple of the LO phonon energy, the conductivity approaches Drude-like behavior slowly.

Time-resolved investigation of the relaxation dynamics after photoexcitation, measured by optical pump terahertz-probe spectroscopy, allows us to study the various scattering processes affected by the carrier scattering rate and carrier density. The carrier density changes within a picosecond timescale are related to various relaxation processes such as surface recombination occurring usually within the sub-picosecond timescale and bulk recombination and diffusion within a much longer timescale (several hundreds of picoseconds). From the time-resolved terahertz transmission studies of semiconductors such as GaAs and InP irradiated by various photon energies, the photoexcited carrier dynamics can be characterized by providing the time-resolved, frequency-dependent photoconductivity of the semiconductors, in terms of pump photon energies as shown in Figure 2.

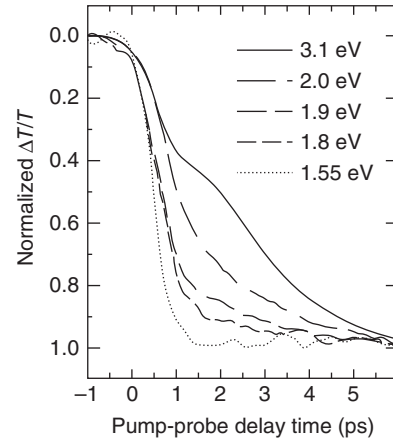

Figure 2 Optical pump terahertz-probe time-resolved measurement of GaAs (100) under different pump photon energies. With higher pump photon energies, photoexcited electrons can access the satellite valleys having lower mobility. Source: From M. C. Beard, G. M. Turner, and C. A. Schmuttenmaer, "Transient photoconductivity in GaAs as measured by time-resolved terahertz spectroscopy," Phys. Rev. B 62(23), 15764–15777 (2000). © 2000 American physical society [25].

2.2 Ultrafast Carrier Dynamics in Nanostructured Semiconductors

Terahertz waves have shown substantial promise in many applications, including the critical advantages that one can directly

observe with transient carrier dynamics and conductivity changes [15]. However, it has been still challenging to obtain a reasonable terahertz signal from nanoscale samples directly with typical signal-to-noise detection levels [28]. This is primarily due to the mismatch in the relatively large terahertz spot size (~1 mm) and the nanoscale size of the objects to be detected. Therefore, there remains a huge lack of fundamental understanding regarding the interaction of terahertz radiation with individual nanostructures. Metamaterials can potentially be used to increase the detection sensitivity through strong localization and enhancement of the incident terahertz electromagnetic field (will be discussed in detail in Section 3.2). To investigate the carrier dynamics of nanostructured semiconductors, ultrafast optical measurements have been performed mostly on nanowires in ensemble status [29, 30] and thin films [31, 32] under high-power laser-based systems to obtain reasonably sufficient signals. Both ultrafast dynamics and frequency-dependent complex dielectric properties and terahertz conductivity of photoexcited semiconductor nanostructures are introduced in this section. As introduced in some recent studies, the terahertz optical properties and dynamics revealed different behaviors from those of nanostructures in contrast with bulk semiconductors. Here, it is noted that the considered structure dimension is between micrometer and nanometer scales, not covering the quantum regime.

To characterize the carrier dynamics of nanostructured semiconductors, an optical pump excites the nanostructures, and photo-injected carriers inside the nanostructures can be tracked by following a delayed terahertz probe pulse. Terahertz optical response change in film state and nanostructures such as nanowires and nanoparticles can be compared by performing the optical pump terahertz-probe experiment on continuous thin films, nanowire arrays, and mesoporous nanoparticle films (Figure 3a–c). As an example, the studies on carrier dynamics of ZnO nanomaterials are introduced. First of all, the intrinsic optical properties of ZnO nanomaterial films can be measured using a time-resolved terahertz spectroscopy system, which provides a terahertz absorption coefficient, index of refraction, and conductivity [30]. The frequency-dependent terahertz conductivity shows that the films have the highest mobility, followed by nanowires and then nanoparticle films. In addition, the nanostructured ZnO under photoexcitation has similar changes in photoconductivity at short pump-probe delay times, but the nanoparticle films have shorter electron lifetimes that originate from the inherent disorder and the multitude of interfaces in the nanoparticle films (Figure 3d, e).

Another example shows the pump-induced change in peak-transmitted terahertz electric field ($\Delta T/T$) for different pump and probe delay t, for GaAs nanowires (Figure 4). The most striking difference in the measured terahertz field change between bulk and nanowires is exponential decay trends. The observed conductivity dynamics for GaAs nanowires differ from those for bulk GaAs, showing ultrashort (300 fs) lifetimes due to charge trapping at the nanowire surface. A higher surface-to-volume ratio in such nanostructures provides higher trap density at the nanowire surface.

In thin films, transient terahertz optical response to photoexcitation can be studied in a single layer of MoS_2 and WSe_2 [31] and graphene [32, 33]. Using a combined system of photoluminescence (PL) and terahertz conductivity spectroscopy, ultrafast charge carrier dynamics in monolayers and trilayers of transition metal dichalcogenides (TMDCs) MoS_2 and WSe_2 were measured. Photoconductivity and PL response time of just 350 fs for chemical vapor deposition (CVD)-grown monolayer MoS_2 and 1 ps for trilayer MoS_2 and monolayer WSe_2 were recorded, implying ultrafast modulation and switching available [31]. In epitaxial graphene, the first-time measurement

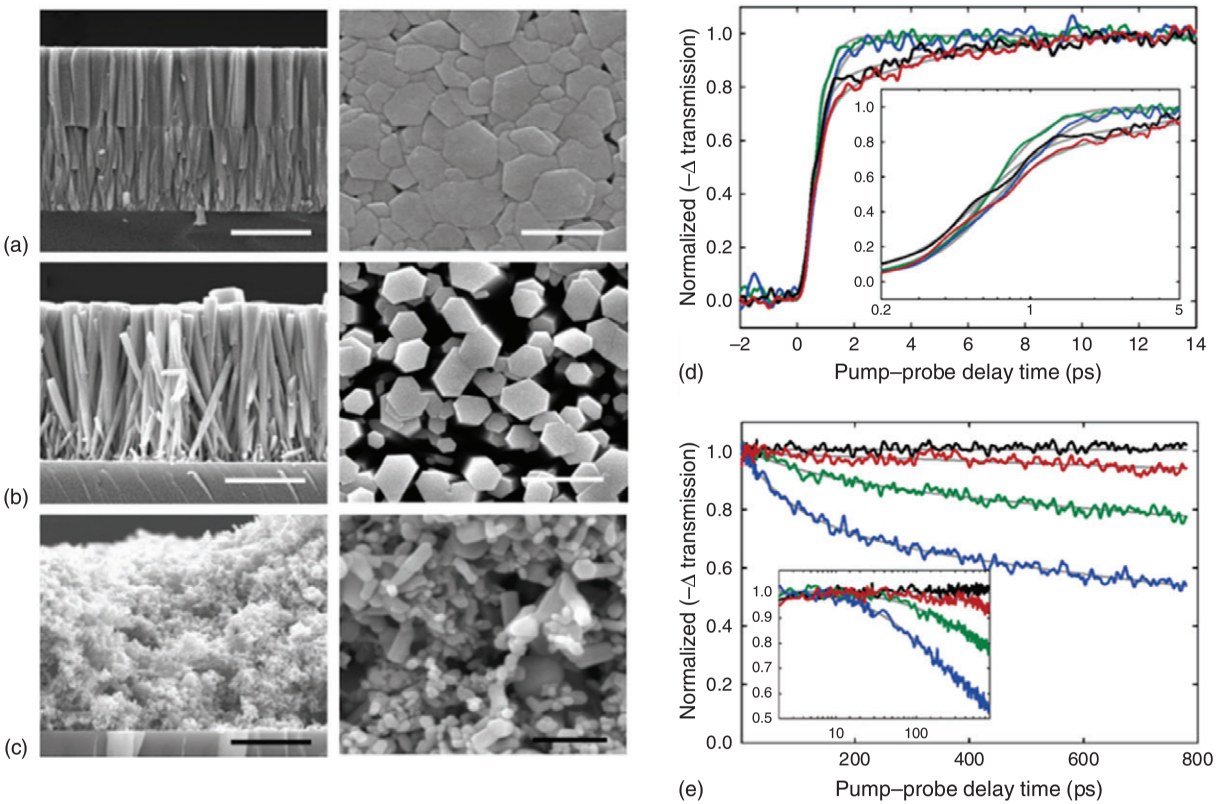

Figure 3 Cross-sectional (left) and top view (right) images of scanning electron microscope for ZnO continuous thin film (a), nanowire array (b), and mesoporous nanoparticle film (c). (Scale bars are 2 μm in cross-sectional images, 1 μm in top view images for (a) and (b), and 500 nm in the top view image for (c). Normalized change in transmission as a function of pump-probe delay time, showing (d) electron photo-injection at short times and (e) decay in electron density over long times for the various types of ZnO nanomaterials. Traces for films with ~1-μm grains (black), films with ~500-nm grains (red), nanowires (green), and nanoparticles (blue). Insets represent log-plots. Source: From J. B. Baxter and C. A. Schmuttenmaer, "Conductivity of ZnO Nanowires, Nanoparticles, and Thin Films Using Time-Resolved Terahertz Spectroscopy," J. Phys. Chem. B 110(50), 25229–25239 (2006). © 2006 American chemical society [30].

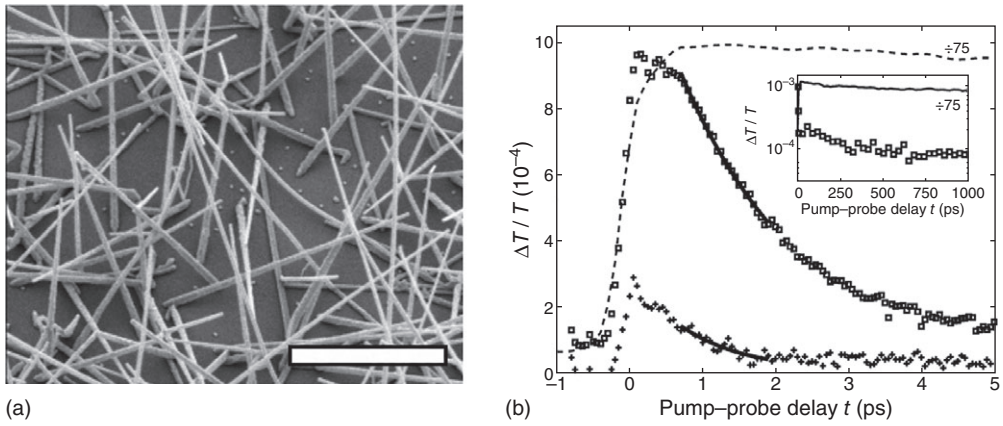

Figure 4 Scanning electron microscope image of GaAs nanowires on a quartz substrate (a). The scale bar is 2 μm. (b) Pump-induced terahertz field change for different pump-probe delays, for GaAs nanowires excited at 800-nm wavelength with an incident pump fluence of 44 μJ cm^{-2} (crosses), and 1.3 mJ cm^{-2} (squares). The dashed line is for bulk GaAs at 1.3 mJ cm^{-2} but reduced in scale by a factor of 75. Source: From P. Parkinson, J. Lloyd-Hughes, Q. Gao, H. H. Tan, C. Jagadish, M. B. Johnston, and L. M. Herz, "Transient Terahertz Conductivity of GaAs Nanowires," Nano Lett. 7(7), 2162–2165 (2007). © 2007 American chemical society [29].

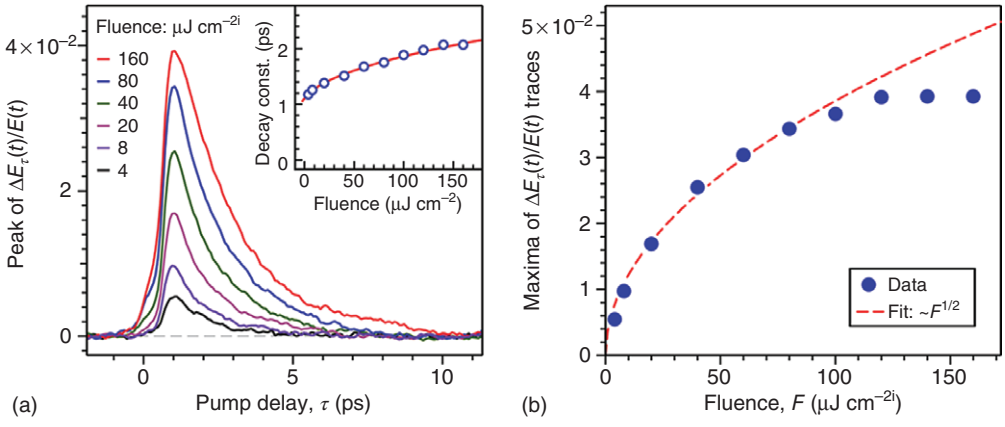

Figure 5 Transient terahertz transmission of photoexcited graphene layer: (a) temporal evolution of the change in the maxima of the transmitted terahertz signal, for different pump fluences. (b) Maxima of the time traces as a function of applied fluence, which saturates at higher fluences. Source: From G. Jnawali, Y. Rao, H. Yan, and T. F. Heinz, "Observation of a Transient Decrease in Terahertz Conductivity of Single-Layer Graphene Induced by Ultrafast Optical Excitation," Nano Lett. 13(2), 524–530 (2013). © 2013 American chemical society [33].

of inter-band electron–hole recombination rates represents that carrier cooling occurs on sub-picosecond timescales [32]. Different pump pulse energy experiments show that the recombination rates are carrier-density dependent. A recent work studied the frequency-dependent sheet conductivity of graphene grown by CVD [33]. Figure 5 presents the change in the maxima of terahertz waveforms under different pump fluences. The measured terahertz transmission increases as photoexcitation fluence increases on the timescale of 1 ps, exactly corresponding to a photoinduced decrease in the terahertz conductivity. This counterintuitive result is explained by the

fact that the Drude weight is a nonlinear function of the electronic temperature [34]. The Drude weight is more important at relatively high pump fluence, resulting in an increase in the graphene conductivity, which would compensate for the decrease in the conductivity induced by an increased electron scattering rate.

Carrier lifetime can be changed in accordance with the surface and interface states of the nanostructures. In nanoscale materials with higher surface-to-volume, higher trap density at the surface induces faster charge trapping and relaxation time. Also, photoexcitation induces an increase in electron density, causing highest mobility in nanostructures than in homogenous films. The interesting results in photoconductive response with different optical pump fluences were introduced in various mono-layered thin films as TMDCs and graphene. A more efficient way to investigate such interesting optical responses in nanoscale materials, without completely new fabrication or growth using such advanced technologies, will be introduced in the next section.

3 Terahertz Nanoscopy Using Metallic Nanostructures

3.1 Field Confinement and Enhancement in Metallic Nanostructures

As one of the candidates confining electrical charges strongly at local sites, metallic nanogaps, composed of two thin metal structures with a gap in nanoscale, can be considered. The metallic nanogaps confine and enhance the electric field of incident electromagnetic waves inside and near the gap due to the charge accumulation around the sharper edges of the metal as shown in Figure 6a [35–38]. In long-wavelength waves such as terahertz waves and microwaves, the electric field is completely concentrated at the gap because of the high contrast of dielectric constant, due to which all electromagnetic waves squeeze through the gap. This means that field enhancements in gaps much smaller than the wavelength become stronger when the gaps become narrower. In a 2009 report, enhancement of a terahertz electric field was achieved by a slit of width around 30 000 times smaller than the wavelength [35]. A single nanoslit with a width of 70 nm and a length of 3 mm was fabricated in a 60-nm-thick gold film by a focused ion beam (Figure 6b). In the report, the transmitted amplitude of the terahertz electric field through the narrow slit was much larger than the ratio of the area covered by the gap (Figure 6c), implying a 1000 field enhancement inside the slit (Figure 6d).

One-dimensional slit structure provides a strong local electric field with resonance-less $1/f$ frequency dependence [35, 39–41]. Strong field enhancement at a specific wavelength can be also achieved by rectangular holes that have a nanoscale width but a few hundred micrometric lengths [39, 42, 43] (Figure 7). These rectangular holes are tailored to work as resonators, slot antennas in the terahertz frequency range. The resonance conditions are tuned by both shapes of a single structure and distance between the structures [42–47]. The strong resonance behavior of diverse terahertz metallic structures has been observed by both far-field transmission and near-field imaging measurements [48].

Metallic gap structures in which terahertz waves are strongly confined and enhanced particularly at the resonance condition have been exploited for applications of terahertz technology such as switching devices, molecular sensing, and so on [49–54]. The main idea is based on the enhanced interaction between strong localized electromagnetic waves and matters positioned around the metallic gap as well as inside the gap. In particular, a localized strong field near the metallic gap leads to strong light absorption by small molecules, polymers, oxides, and semiconductor materials, which enables single-molecule studies, nanoscale lithography, and nanoscale physics in diverse

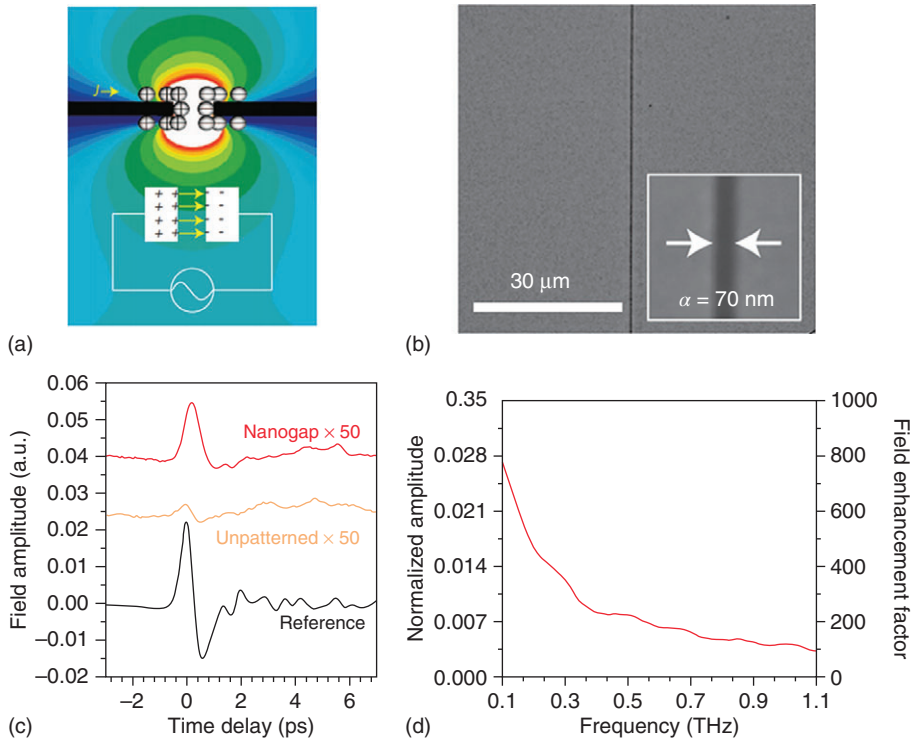

Figure 6 (a) Electric field, *E*, induced current density, *J*, and accumulated charge distributions near the metallic nanogap illuminated with terahertz waves. (b) Scanning electron microscope image 70-nm-wide metal gap fabricated by focused ion beam machining. (c) Terahertz electric fields transmitted through 70-nm-wide metal gap (red), unpatterned gold film (yellow), and 2 mm by 2 mm aperture as a reference (black) in the time domain. (d) Normalized transmitted amplitude and electric field enhancement for 70-nm-wide gaps. Source: From M. A. Seo, H. R. Park, S. M. Koo, D. J. Park, J. H. Kang, O. K. Suwal, S. S. Choi, P. C. M. Planken, G. S. Park, N. K. Park, Q. H. Park, and D. S. Kim, "Terahertz field enhancement by a metallic nano slit operating beyond the skin-depth limit," Nat. Photonics 3(3), 152–156 (2009). © 2009 Springer nature [35].

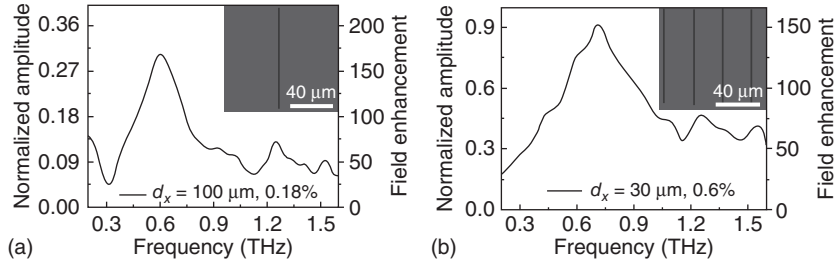

Figure 7 Normalized transmitted amplitude and electric field enhancement spectra for arrays of terahertz nanoslot antennas with a length of 100 μm, a width of 200 nm, periods of 100 μm (a) and 30 μm (b). Source: From H. R. Park, Y. M. Park, H. S. Kim, J. S. Kyoung, M. A. Seo, D. J. Park, Y. H. Ahn, K. J. Ahn, and D. S. Kim, "Terahertz nanoresonators: Giant field enhancement and ultrabroadband performance," Appl. Phys. Lett. 96(12), 121106 (2010). © 2010 AIP Publishing [42].

materials. Complementary structures to the nanogaps, metallic tip type structures, triggering strong electrical charge accumulation at extremely small sites [55] with an application example like the nanotomography [56] can be also considered. Near-field scanning optical microscopy with the metallic tip was combined to the terahertz spectroscopy for terahertz studies in nanoscale, allowing ultrafast spectroscopy with 10-fs time resolution on 10-nm-scale nanoparticles [20, 57].

3.2 Metallic Nanogaps for Surface Carrier Dynamics in Semiconductors

Separating the surface carrier dynamics from bulk and grain-boundary recombination in semiconductor materials has been challenging. To probe the effect of different surface properties of semiconductor materials on photoexcited carrier dynamics, one can use nanosized materials such as nanofilms, nanowires, and nanoparticles, which have a very large surface-to-volume ratio [29, 58, 59]. Another approach to selectively probe the surface properties of bulk semiconductors in pump-probe techniques is using shorter wavelength electromagnetic waves as a probe beam, which has a much smaller penetration depth [60]. However, this approach makes it inevitable to use large photon energy, which can lead to ionization and material breakdown.

On the other hand, electromagnetic waves localized by metallic nanogaps can efficiently interact with the surface state of bulk materials on which the metallic nanogaps are patterned. Particularly, in the optical pump terahertz-probe spectroscopy technique, the optical pump beam of infrared light can generate photoexcited carriers near the surface because of its confinement by metal nanogaps. In addition, the terahertz probe beam is even more strongly confined and enhanced, resulting in sensitive detection by enhanced absorption as well as surface probing of bulk materials by strong confinement behavior near the surface. In 2017, a new nanoscopy technique for surface probing of bulk semiconductor materials was suggested by patterning metal nanogaps on target materials [61, 62]. Figure 8 shows the time-resolved transient transmission change of terahertz waves by photoexcited carriers of SI-InP and SI-GaAs in which metallic gaps are patterned, respectively. Note that the thickness of InP and GaAs is 500 μm. Compared to the time-resolved data of an unpatterned semiconductor that shows a longer carrier lifetime up to several hundreds of picoseconds (gray and black lines), the metal-patterned semiconductors render shorter carrier lifetimes down to a picosecond scale for the nanoscale metal-gap-patterned case. Carrier lifetime for 35-nm-gap-patterned GaAs reached down to ~2 ps, which is close to the limit of terahertz time resolution.

The faster carrier lifetime of nanopatterned semiconductors is explained by surface carrier dynamics of bulk semiconductors, originating from band bending effect by the energy of surface states due to dangling bonds. Strong confinement of two electromagnetic waves (terahertz probe beam and infrared pump beam) near the surface accompanied by metallic nanogaps enables the direct observation of the surface state of bulk materials. Figure 9a presents the calculated intensity distribution of terahertz probe beam (top) and optical pump beam (bottom) for 50-nm metal-gap-patterned InP, showing that both pump and probe beams are strongly confined near the metal gap with even stronger field confinement for a longer wavelength of electromagnetic waves ($\lambda_{pump} \sim 800$ nm and $\lambda_{probe} \sim 600$ μm). From the near-field distributions of two electromagnetic waves, the effective pump depth and probe depth can be defined by the full width at half maximum value at which optical power drops to $1/e$ from the surface value. With the decreasing gap size, as shown in Figure 9b, the effective penetration depth of the pump beam maintains the value of the intrinsic penetration depth of semiconductors (~300 nm for InP and

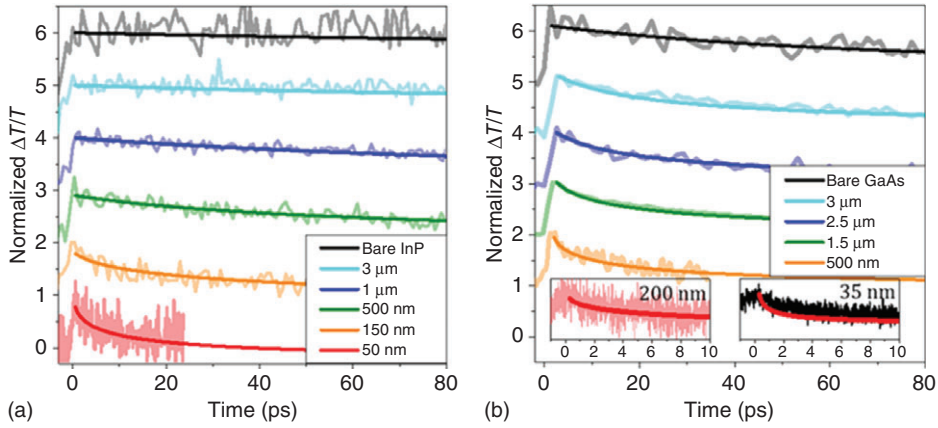

Figure 8 Normalized terahertz transmission changes of metal-patterned bulk InP (a) and GaAs (b) as a function of pump-probe delay time. The metal gap size is varied from a 3 μm to a few tens of nanometer scale. Each measured time-resolved data was fitted with the values of surface recombination velocity $S = 1.5 \times 10^5$ cm s^{-1}, diffusion coefficient $D = 0.3$ cm^2 s^{-1} for InP (a) and $S = 1.1 \times 10^6$ cm s^{-1}, $D = 45$ cm^2 s^{-1} for GaAs (b). Source: From G. Choi, Y.-M. Bahk, T. Kang, Y. Lee, B. H. Son, Y. H. Ahn, M. Seo, and D.-S. Kim, "Terahertz Nanoprobing of Semiconductor Surface Dynamics," Nano Lett. 17(10), 6397–6401 (2017). © 2017 American Chemical Society [61].

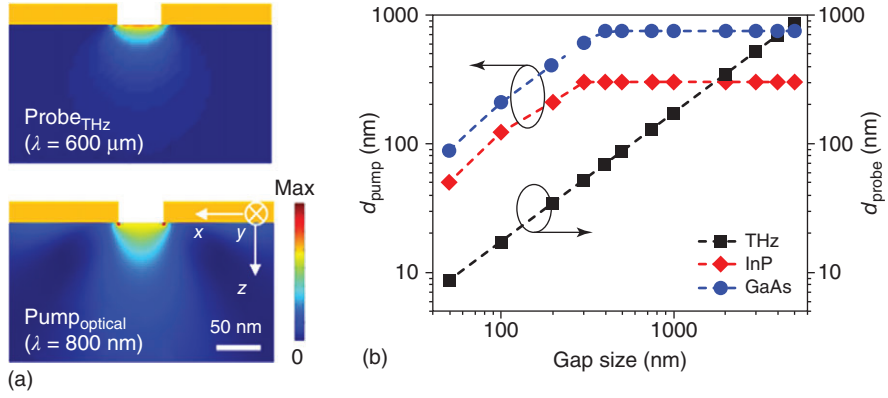

Figure 9 (a) Intensity $|E_x^2|$ distribution of terahertz probe beam (top) and Poynting vector $|S|$ distribution of optical pump beam (bottom) near 50 -nm-wide metal gap patterned on InP, respectively. (b) Effective pump depth d_{pump} of optical pump beam for InP (red dot) and GaAs (blue dot) and effective probe depth d_{probe} of terahertz probe beam (black dot) as a function of gap size. Source: From G. Choi, Y.-M. Bahk, T. Kang, Y. Lee, B. H. Son, Y. H. Ahn, M. Seo, and D.-S. Kim, "Terahertz Nanoprobing of Semiconductor Surface Dynamics," Nano Lett. 17(10), 6397–6401 (2017). © 2017 American chemical society [61].

~750 nm for GaAs) and then decreases down to sub-100-nm scale. This smaller pump depth by confinement behavior of the optical pump beam leads that carriers are dominantly excited within the depth smaller than the intrinsic penetration depth. On the other hand, the effective probe depth defined by confinement of the terahertz probe beam linearly decreases down to a few tens of nanoscale even smaller than the pump depth, which implies that one can sensitively capture the surface-only carrier dynamics invisible in unpatterned semiconductors. Controlling the pump and probe depth by the gap size enables selective detection of surface carrier dynamics of bulk semiconductors.

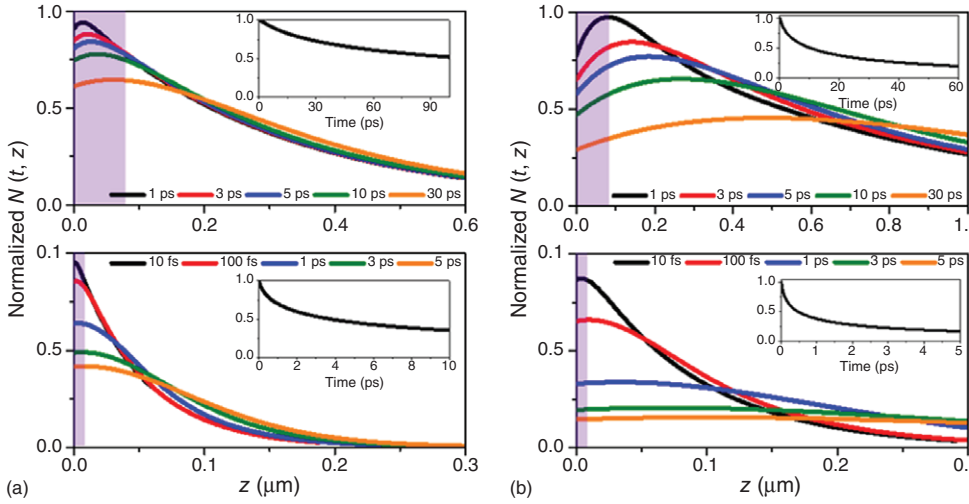

Figure 10 Normalized carrier density N as a function of distance z from the surface for 500 nm (top) and 50 nm (bottom) gap-patterned InP (a) and GaAs (b), at five different time delays. In the calculation, the values of $S = 1.5 \times 10^5$ cm s^{-1}, $D = 0.3$ cm^2 s^{-1} for InP and $S = 1.1 \times 10^6$ cm s^{-1}, $D = 45$ cm^2 s^{-1} for GaAs were used. The violet shades represent the effective probe depth d_{probe} controlled by terahertz confinement and the insets show N integrated from the surface to d_{probe} as a function of time. Source: From G. Choi, Y.-M. Bahk, T. Kang, Y. Lee, B. H. Son, Y. H. Ahn, M. Seo, and D.-S. Kim, "Terahertz Nanoprobing of Semiconductor Surface Dynamics," Nano Lett. 17(10), 6397–6401 (2017). © 2017 American chemical society [61].

Surface properties of bulk semiconductors are quantitatively described by surface recombination velocity S and diffusion coefficient D that can be extracted from the time-resolved data of metal-patterned semiconductors (Figure 10). At first, the normalized photoexcited carrier density N is expressed as follows:

$$N(t,z) = \frac{1}{2}\exp\left(-\frac{z^2}{4Dt}\right) \times \left[w\left(\alpha_{\text{eff}}\sqrt{Dt} - \frac{z}{2\sqrt{Dt}}\right) - \frac{S+\alpha_{\text{eff}}\sqrt{Dt}}{S-\alpha_{\text{eff}}\sqrt{Dt}} w\left(\alpha_{\text{eff}}\sqrt{Dt} + \frac{z}{2\sqrt{Dt}}\right) + \frac{2S}{S-\alpha_{\text{eff}}D} w\left(S\sqrt{\frac{t}{S}} + \frac{z}{2\sqrt{Dt}}\right)\right]$$

where t is the delay time, z is a distance from the surface, α_{eff} is the absorption coefficient at the excitation wavelength, and $w(\zeta) = \exp(\zeta^2)[1 - \text{erf}(\zeta)]$. The absorption coefficient α required for the definition of the photoexcited carrier depth is replaced by the effective absorption coefficient α_{eff} corresponding to an inverse of effective pump depth d_{pump} in the nanopatterned semiconductor. As shown in Figure 10, normalized carrier density N as a function of distance z from the surface for the metal-patterned semiconductor can be calculated at each time delay with fitting parameters S and D. At each time delay t, the terahertz transmission reduction in metal-patterned semiconductors is determined by the carrier densities integrated from the surface to the effective probe depth d_{probe} controlled by the gap size. Finally, because the transmission reduction $\Delta T/T$ is proportional to the change of carrier density, the time-resolved data is fitted by the calculated normalized carrier density integrated within the effective probe depth as a function of time, leading to the extraction of the surface properties S and D. For instance, Figure 10 shows $N(z)$ for 500-nm (top) and 50-nm (bottom) gap-patterned InP (a) and GaAs (b) at five different time delays with the values of

$S = 1.5 \times 10^5$ cm s^{-1}, $D = 0.3$ cm^2 s^{-1} for InP and $S = 1.1 \times 10^6$ cm s^{-1}, $D = 45$ cm^2 s^{-1} for GaAs. The insets of the figure display the normalized carrier density integrated within the effective probe depth (violet shades) as a function of time, which is well fitted with the time-resolved data as shown in Figure 8. This process of the metal-gap-based surface probing technique provides the direct observation of the surface carrier dynamics of bulk semiconductors.

4 Summary and Outlook

In this article, we surveyed studies on photoinduced carrier dynamics of semiconductors including bulk materials and nanomaterials such as thin films, nanowires, and nanoparticles. The experimental tool was focused on femtosecond laser-based optical pump terahertz-probe spectroscopy, which is an excellent technique for studying the transient photoconductivity of semiconductors under photoexcitation because it allows us to measure the complex-valued, frequency-dependent photoconductivity in picoseconds and sub-picosecond timescales. One of the promising optical phenomena observed in photoexcited semiconductor nanomaterials is surface carrier dynamics owing to the high surface-to-volume ratio of nanostructures. Compared to bulk materials, carrier dynamics of semiconductor nanomaterials have a faster decaying time, originated from trapping and fast recombination at surfaces and interfaces of nanomaterials. Here, two approaches to examine the surface carrier dynamics of semiconductors by overcoming the diffraction limit of terahertz waves were introduced: (i) preparing the large area film state with the nanomaterials (nanowires or nanoparticles) in ensemble statue [29–32, 58, 59] and (ii) patterning the metallic nanogaps on bulk materials to confine the terahertz waves in a nanosized volume [61, 62]. In particular, metal nanostructures facilitating strong light–matter interaction provide surface nanoprobing of bulk materials with high sensitivity due to their ability to localize and enhance the electromagnetic waves in nanoscale. Further developments of ultrafast nanoprobing using terahertz waves will require the improvement in spatiotemporal resolutions and advances in nanolithography and synthesis of nanomaterials.

Related Articles

THz Time-Domain Spectroscopy Techniques for Cultural Heritage
Strong Light-Matter Interaction
Optoelectronics
Ultrafast Spectroscopy
Surfaces and Interfaces of Solids, Structure of
Semiconductors, Compound–Material Properties
Wave Optics
Nonlinear Optics
Optical Properties of Solids

References

1 Fattinger, C. and Grischkowsky, D. (1989). *Appl. Phys. Lett.* 54 (6): 490–492.
2 van Exter, M., Fattinger, C., and Grischkowsky, D. (1989). *Opt. Lett.* 14 (20): 1128.
3 Grischkowsky, D., Keiding, S., van Exter, M., and Fattinger, C. (1990). *J. Opt. Soc. Am. B* 7 (10): 2006.
4 Fattinger, C. and Grischkowsky, D. (1988). *Appl. Phys. Lett.* 53 (16): 1480–1482.
5 van Exter, M. and Grischkowsky, D. (1990). *Phys. Rev. B* 41 (17): 12140–12149.
6 Fischer, B.M., Walther, M., and Jepsen, P.U. (2002). *Phys. Med. Biol.* 47 (21): 3807–3814.

7 Duvillaret, L., Garet, F., and Coutaz, J.-L. (1996). *IEEE J. Sel. Top. Quantum Electron.* 2 (3): 739–746.
8 Duvillaret, L., Garet, F., and Coutaz, J.-L. (1999). *Appl. Opt.* 38 (2): 409.
9 Walther, M., Plochocka, P., Fischer, B. et al. (2002). *Biopolymers* 67 (4–5): 310–313.
10 Mittleman, D.M., Jacobsen, R.H., Neelamani, R. et al. (1998). *Appl. Phys. B Lasers Opt.* 67 (3): 379–390.
11 Fitzgerald, A.J., Cole, B.E., and Taday, P.F. (2005). *J. Pharm. Sci.* 94 (1): 177–183.
12 Stoik, C.D., Bohn, M.J., and Blackshire, J.L. (2008). *Opt. Express* 16 (21): 17039.
13 Jackson, J.B., Mourou, M., Whitaker, J.F. et al. (2008). *Opt. Commun.* 281 (4): 527–532.
14 Yamamoto, K., Yamaguchi, M., Miyamaru, F. et al. (2004). *Jpn. J. Appl. Phys.* 43 (3B): L414–L417.
15 Ulbricht, R., Hendry, E., Shan, J. et al. (2011). *Rev. Mod. Phys.* 83 (2): 543–586.
16 Zielbauer, J. and Wegener, M. (1996). *Appl. Phys. Lett.* 68 (9): 1223–1225.
17 Breusing, M., Ropers, C., and Elsaesser, T. (2009). *Phys. Rev. Lett.* 102 (8): 086809.
18 Breusing, M., Kuehn, S., Winzer, T. et al. (2011). *Phys. Rev. B* 83 (15): 153410.
19 Yuma, B., Berciaud, S., Besbas, J. et al. (2013). *Phys. Rev. B* 87 (20): 205412.
20 Eisele, M., Cocker, T.L., Huber, M.A. et al. (2014). *Nat. Photonics* 8 (11): 841–845.
21 Poellmann, C., Steinleitner, P., Leierseder, U. et al. (2015). *Nat. Mater.* 14 (9): 889–893.
22 Vengurlekar, A.S. and Jha, S.S. (1987). *Appl. Phys. Lett.* 51 (5): 323–325.
23 Binder, R. and Koch, S.W. (1995). *Prog. Quantum Electron.* 19 (4–5): 307–462.
24 Nikolić, B.K., Souma, S., Zĝrbo, L.P., and Sinova, J. (2005). *Phys. Rev. Lett.* 95 (4): 1–4.
25 Beard, M.C., Turner, G.M., and Schmuttenmaer, C.A. (2000). *Phys. Rev. B* 62 (23): 15764–15777.
26 Vengurlekar, A.S. and Jha, S.S. (1988). *Phys. Rev. B* 38 (3): 2044–2056.
27 Vengurlekar, A.S. and Jha, S.S. (1989). *J. Appl. Phys.* 65 (8): 3189–3196.
28 O'Hara, J.F., Singh, R., Brener, I. et al. (2008). *Opt. Express* 16 (3): 1786.
29 Parkinson, P., Lloyd-Hughes, J., Gao, Q. et al. (2007). *Nano Lett.* 7 (7): 2162–2165.
30 Baxter, J.B. and Schmuttenmaer, C.A. (2006). *J. Phys. Chem. B* 110 (50): 25229–25239.
31 Docherty, C.J., Parkinson, P., Joyce, H.J. et al. (2014). *ACS Nano* 8 (11): 11147–11153.
32 George, P.A., Strait, J., Dawlaty, J. et al. (2008). *Nano Lett.* 8 (12): 17–20.
33 Jnawali, G., Rao, Y., Yan, H., and Heinz, T.F. (2013). *Nano Lett.* 13 (2): 524–530.
34 Gusynin, V.P., Sharapov, S.G., and Carbotte, J.P. (2009). *New J. Phys.* 11 (9): 095013.
35 Seo, M.A., Park, H.R., Koo, S.M. et al. (2009). *Nat. Photonics* 3 (3): 152–156.
36 Muhlschlegel, P. (2005). *Science* 308 (5728): 1607–1609.
37 Tamaru, H., Kuwata, H., Miyazaki, H.T., and Miyano, K. (2002). *Appl. Phys. Lett.* 80 (10): 1826–1828.
38 Fromm, D.P., Sundaramurthy, A., Schuck, P.J. et al. (2004). *Nano Lett.* 4 (5): 957–961.
39 Lee, J.W., Seo, M.A., Kang, D.H. et al. (2007). *Phys. Rev. Lett.* 99 (13): 137401.
40 Kang, J.H., Kim, D.S., and Park, Q.-H. (2009). *Phys. Rev. Lett.* 102 (9): 093906.
41 Bahk, Y.M., Han, S., Rhie, J. et al. (2017). *Phys. Rev. B* 95 (7): 1–5.
42 Park, H.R., Park, Y.M., Kim, H.S. et al. (2010). *Appl. Phys. Lett.* 96 (12): 121106.
43 Park, H.R., Koo, S.M., Suwal, O.K. et al. (2010). *Appl. Phys. Lett.* 96 (21): 2008–2011.
44 Lee, J., Seo, M., Park, D. et al. (2006). *Opt. Express* 14 (3): 1253–1259.
45 Bahk, Y.M., Park, H.R., Ahn, K.J. et al. (2011). *Phys. Rev. Lett.* 106 (1): 013902.
46 Park, H.-R., Bahk, Y.-M., Ahn, K.J. et al. (2011). *ACS Nano* 5 (10): 8340–8345.
47 Kang, J.H., Choe, J.-H., Kim, D.-S., and Park, Q.-H. (2009). *Opt. Express* 17 (18): 15652–15658.

48 Knab, J.R., Adam, A.J.L., Nagel, M. et al. (2009). *Opt. Express* 17 (17): 15072.
49 Seo, M., Kyoung, J., Park, H. et al. (2010). *Nano Lett.* 10 (6): 2064–2068.
50 Kyoung, J., Seo, M., Park, H. et al. (2010). *Opt. Express* 18 (16): 16452.
51 Choi, S.B., Kyoung, J.S., Kim, H.S. et al. (2011). *Appl. Phys. Lett.* 98 (7): 071105.
52 Jeong, Y.-G., Bernien, H., Kyoung, J.-S. et al. (2011). *Opt. Express* 19 (22): 21211.
53 Park, H.-R., Ahn, K.J., Han, S. et al. (2013). *Nano Lett.* 13 (4): 1782–1786.
54 Jeong, Y.-G., Paul, M.J., Kim, S.-H. et al. (2013). *Appl. Phys. Lett.* 103 (17): 171109.
55 Chen, X., Hu, D., Mescall, R. et al. (2019). *Adv. Mater.* 31: 1804774.
56 Govyadinov, A.A., Mastel, S., Golmar, F. et al. (2014). *ACS Nano* 8 (7): 6911–6921.
57 Huber, A.J., Keilmann, F., Wittborn, J. et al. (2008). *Nano Lett.* 8 (11): 3766–3770.
58 Calarco, R., Marso, M., Richter, T. et al. (2005). *Nano Lett.* 5 (5): 981–984.
59 Li, M., Wu, B., Ekahana, S.A. et al. (2012). *Appl. Phys. Lett.* 101 (9): 091104.
60 Sabbah, A.J. and Riffe, D.M. (2002). *Phys. Rev. B* 66 (16): 165217.
61 Choi, G., Bahk, Y.-M., Kang, T. et al. (2017). *Nano Lett.* 17 (10): 6397–6401.
62 Choi, G., Kang, T., Seo, M. et al. (2018). *ACS Photonics* 5 (12): 4739–4744.